Available online at www.sciencedirect.com
SCIENCE DIRECT®
Nuclear Instruments and Methods in Physics Research A 556 (2006) 516–526
NUCLEAR INSTRUMENTS & METHODS IN PHYSICS RESEARCH Section A
www.elsevier.com/locate/nima

The Ring Counter (RCo): A high resolution IC–Si–CsI(Tl) device for heavy ion reaction studies at 10–30 MeV/A

A. Moroni[a], M. Bruno[b], L. Bardelli[c], S. Barlini[d], S. Brambilla[a], G. Casini[c], R. Cavaletti[b], M. Chiari[c], A. Cortesi[a], M. D'Agostino[b,*], J. De Sanctis[b], E. Geraci[b], G. Giordano[e], A. Giussani[a], F. Gramegna[d], B. Guiot[b], V. Kravchuk[d], A. Lanchais[d], G.V. Margagliotti[f], A. Nannini[c], A. Ordine[e], S. Piantelli[c], G. Vannini[b], L. Vannucci[d]

[a]*Istituto Nazionale di Fisica Nucleare, Sezione di Milano and Dipartimento di Fisica dell'Università, Milano, Italy*
[b]*Istituto Nazionale di Fisica Nucleare, Sezionedi Bologna and Dipartimento di Fisica dell'Università, Bologna, Italy*
[c]*Istituto Nazionale di Fisica Nucleare, Sezione di Firenze and Dipartimento di Fisica dell'Università, Firenze, Italy*
[d]*Istituto Nazionale di Fisica Nucleare, Laboratori Nazionali di Legnaro, Italy*
[e]*Istituto Nazionale di Fisica Nucleare, Sezione di Napoli and Dipartimento di Fisica dell'Università, Napoli, Italy*
[f]*Istituto Nazionale di Fisica Nucleare, Sezione di Trieste and Dipartimento di Fisica dell'Università, Trieste, Italy*

Received 6 September 2005; received in revised form 24 October 2005; accepted 27 October 2005
Available online 1 December 2005

Abstract

An annular detector (Ring Counter, RCo) is presented, which has been designed and built to detect and identify in mass and charge light charged particles and fragments with very low energy thresholds and high energy resolution. It complements the GARFIELD apparatus, operating at INFN Laboratori Nazionali di Legnaro, to detect the forward emitted products of nuclear heavy ion reactions. It consists of eight sectors of a three-stage telescope, each one formed by an ionization chamber followed by eight strips of a silicon detector and by two CsI(Tl) scintillators. Construction features and performances are described and discussed in details.

PACS: 29.40.Cs; 29.40.Mc; 29.40.Wk; 25.70.Pq

Keywords: Heavy-ion reactions; Ionization chambers; Silicon strip detectors; Charged particle and fragment detection; Fragment isotopic resolution; Isotope correlation functions

1. Introduction

In recent years the study of dynamic and thermodynamic properties of excited systems, formed in heavy ion reactions, has been one of the most investigated items of nuclear physics [1]. In the light of the forthcoming development of exotic beam facilities, the opportunity to deeply explore the third dimension of the nuclear equation of state, the isospin dimension, will finally be opened. However, the experimental scenario of this research line is quite complex. In fact, the goal is to collect the most complete information on the excited nuclear systems at the time of their formation, starting from the observation as more complete as possible of the detected final products at the end of the secondary decay stage. It is then fundamental to obtain knowledge of all the properties of the light particles and fragments at the time they impinge on the detector. Indeed this can allow, through a complete correlation analysis, to trace back the secondary decays.

For this purpose, a new generation of detection devices, as the one proposed by the Eurisol Instrumentation task group [2] is necessary.

The most important requirements for these detecting systems are:

1. mass and charge identification of all the reaction products, from light particles to Intermediate Mass Fragments (IMF) up to evaporation residues;

*Corresponding author. Tel.: +39 051 2091081; fax: +39 051 247244.
E-mail address: dagostino@bo.infn.it (M. D'Agostino).

0168-9002/$ - see front matter © 2005 Elsevier B.V. All rights reserved.
doi:10.1016/j.nima.2005.10.123

2. very low energy thresholds (of the order of few hundreds of keV/A) for both detection and identification of the reaction products;
3. very good energy resolution (of the order of 1%) on a large dynamical range (from a few MeV to some GeV);
4. very high angular precision ($\leqslant 1^\circ$) and 4π coverage of the solid angle with sufficient granularity in order to allow reliable correlation function analyses;
5. dedicated electronics allowing to perform on-line preliminary checks and identification on raw data.

The conceptual design of the detection system proposed by the Eurisol group requires about few thousand telescopes and about 10^4 electronic channels. Of course, the human and financial cost of such an apparatus is unaffordable by an experimental group of a single country: only an European (or worldwide) collaboration would be able to build it. Waiting for this possibility, the easiest (and only) way to get refined and precise information is to improve the existing devices by a limited amount of complementary systems. Thus, these improved devices will fulfill some of the above listed requirements, but only in a limited solid angle covered by a relatively small number of detectors [3,4].

In this paper we describe the so-called Ring Counter (RCo), a device presently coupled to the GARFIELD apparatus [5,6] at the INFN Laboratori Nazionali di Legnaro (LNL). The RCo can also be used together with other ancillary devices, like parallel plates or gamma scintillators [7]. Here we show that this device is suitable for thermodynamic investigations, starting from the liquid side of the caloric curve, of $A \approx 100$ systems formed in heavy ion reactions at moderate incident energies ($\sim$ 10–30 MeV/A), which are the aims of the INFN NUCL-EX collaboration [8–11].

In Section 2 we describe in detail the detectors used in the RCo, while Section 3 is devoted to present its performance. Perspectives and conclusions are presented in Sections 4 and 5, respectively.

2. The device

The Ring Counter (RCo) is an annular detector designed to be centered at 0° with respect to the beam direction. It is an array of three-stage telescopes realized in a truncated cone shape. The first stage is an ionization chamber (IC), the second a strip silicon detector (Si) and the last stage a CsI(Tl) scintillator. Each stage of the RCo is mounted on a low-mass aluminum support that is adjustable, for the relative alignment of all the active elements of the device. A picture of the whole apparatus is shown in Fig. 1.

The RCo is designed to operate in high vacuum ($P \sim 1 \times 10^{-6}$ Torr) with minimal outgassing.

The RCo has eight separate silicon detectors, pie shaped (see Section 2.2), each one segmented into eight independent annular strips on the front surface (junction side), thus

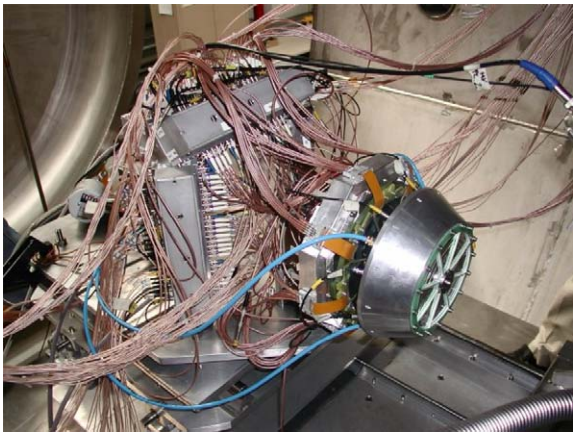

Fig. 1. Picture of the RCo, showing also the sliding plate and the preamplifiers.

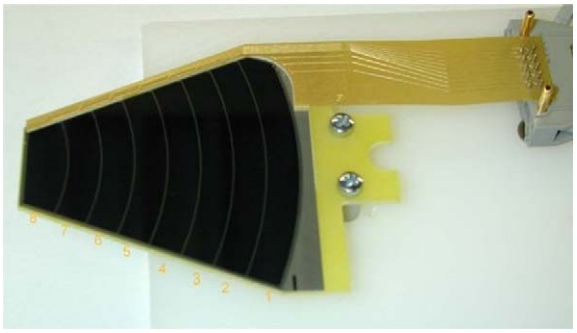

Fig. 2. One of the Si detectors of the RCo. Each one of the eight strips has a size of 8.55 mm. The full length of the silicon detector is 68.4 mm (see Table 1).

increasing the granularity of the detector. The rear surface (ohmic side) consists of an unique electrode. Each strip has a bonding contact to a track in a Kapton ribbon ending with a multiple connector (see Fig. 2), allowing the connection to the preamplifiers.

In front of each silicon detector there is a sector of a specially designed IC (see Section 2.1). Behind each silicon detector there are two 4.0 cm thick CsI(Tl) crystals (see Section 2.3), read out by photodiodes (PD). The geometrical shapes of the CsI crystals has been designed to cover the cone subtended by the IC. Each couple of crystals is related to one sector of the IC and in particular the CsI(Tl) closer to the beam axis covers the angular range of the four inner strips of the Si-detector, while the external CsI(Tl) covers the four outer strips.

The RCo is mounted on a sliding plate that can be moved forward and backward by means of a remote control. The sliding plate can also be rotated to place the RCo at particular θ-angles.

In the forward position the RCo is ready to operate, being inserted in the conical opening of the GARFIELD drift chambers [5,6]. At the angles subtended by the RCo, silicon detectors can suffer rapid radiation damage by

elastically scattered beams. Protecting the detector from the radiation damage is accomplished by inserting passive brass shields in front of the inner silicon strips, according to the grazing angle and the values of the cross-section of the considered reaction. With the sliding plate in the backward position it is also possible to insert a screen to avoid a possible damage during the beam focusing.

In order to minimize the length and the capacitance of the cables and consequently the noise contribution, the preamplifiers [12] are mounted inside the scattering chamber, on the same sliding plate of the RCo; they are placed in metallic boxes which shield them from external fields (see Fig. 1). The preamplifiers are thermally connected to the boxes which are cooled by a simple water cooling system (water temperature about 12 °C), allowing for dispersion of the heat generated by the preamplifiers themselves.

2.1. The ionization chamber

The IC is divided in the azimuthal direction into eight equal detecting sectors. The IC, which is of the axial field type without Frish grid, has been especially designed to minimize the active area loss: its dead regions match the dead zones of the silicon detectors used as second telescope stage. The depth of the active gas region is 6 cm, the entrance and exit windows are aluminized mylar foils, 3 μm thick.

When the RCo is used as forward ring detector, coupled to the GARFIELD apparatus, the IC is very close to the external wall of the GARFIELD drift chamber. Therefore, it has been chosen to bias a middle electrode (1.5 μm thick doubly aluminized mylar) at a given voltage while keeping the entrance and exit windows grounded, in order to have the same electric field with one half of the potential needed for the whole thickness (about 150 V at a pressure of 50 mb of CF_4).

The CF_4 gas, continuously flowing in the chamber, has been chosen because of its high density (0.19 mg/cm^3 at a pressure of 50 mbar and at a temperature of 20 °C) and high drift velocity (10 cm/μs at 1.25 V/cm/Torr). The latter parameter is important to reduce the electron collection time and the electron–positive ion recombination rate.

The pressure inside the chamber is remotely controlled by a newly developed hardware and software system [13]. The gas enters the chamber through a filtering system for oxygen and water vapor suppression. The gas outlet is controlled by a dry root pump and by a valve whose opening is regulated by the control system in order to keep a constant pressure inside the chamber. The gas flow is of the order of 1 std l/min.

Typical working pressures of the IC are in the range 50–200 mbar, depending on the measurements to be performed. In Section 3 we show results obtained with a very low pressure (50 mbar) operation. Indeed one of the goals of the experiment [8], together with the isotopic identification of light charged particles and fragments (up to the oxygen), was to detect with very low energy thresholds heavy residues, formed by the incomplete fusion of the projectile and the target, to measure their kinetic energy and to evaluate (even if with some uncertainties) their charge.

2.2. The silicon detectors

The eight silicon detectors [14] have a trapezoidal shape (see Fig. 2) with dimensions which fit $\frac{1}{8}$ of the total azimuthal angle and match the sectors of the IC.

Each silicon detector is mounted on a stesalit™ [15] frame, designed to minimize the dead areas and to allow an easy mounting and dismounting of single parts. The eight silicon detectors are mounted on an octagonal stesalit™ frame, which is screwed on the CsI(Tl) holder.

The front surface (junction side) of each silicon detector is segmented into eight strips, which cover the polar angle regions quoted in Table 1, when the RCo is at the measuring position, at 270 mm from the target, corresponding to the minimal distance allowed by the mechanical structure of the Garfield chamber [6]. In Table 1 the internal and external radii of all the eight strips are also presented. The most internal strip is limited by a linear border, as visible in Fig. 2.

The covered polar angles run from 3.5° to 17.5° (see Table 1), corresponding to a solid angle of about 0.27 sr. The angular resolution of each strip is $\Delta\theta \sim \pm 0.9^\circ$ and the geometrical coverage of the Si detector is about 90%. The inactive area is due to the interstrip regions (about 220 μm wide), containing the guard rings all around the strips. The guard rings have to be properly biased, in order to minimize the effects due to the field distortion in the inter-strip region. This strongly reduces the charge split and the cross-talk between contiguous strips, keeping them to about 0.5% and therefore almost negligible. Another inactive area is the printed circuit board frame that holds each Silicon sector, which extends about 3.2 mm beyond the physical dimension of the sector and provides the voltage supply and the extraction of the signals.

Table 1
Radii and polar angle limits of RCo silicon strips

Strip	Int. radius (mm)	Ext. radius (mm)	Min. angle (deg)	Max. angle (deg)
1	76.7	85.0	15.8	17.5
2	68.1	76.4	14.1	15.8
3	59.5	67.9	12.4	14.1
4	50.9	59.3	10.7	12.4
5	42.4	50.7	8.9	10.6
6	33.8	42.1	7.1	8.9
7	25.2	33.6	5.3	7.1
8	16.6	25.0	3.5	5.3

The bulk resistivity of the detector is $\rho = 16\,200\,\Omega\,\mathrm{cm}$, the typical depletion voltage is 40 V and the reverse current of each strip is about 20 nA.

The junction window thickness is thinner than 50 nm and is therefore negligible as far as the energy loss of the particle is concerned. The ohmic window thickness has been kept thinner than 1.5 μm, thus allowing for rather low thresholds also in the reverse mounting configuration. This configuration, where particles enter through the low field side and produce slower electric signals, should help the possibility of charge identification via pulse-shape techniques [16].

The thickness of the silicon detectors is around 300 μm, as stated by the manufacturer. Therefore the energy thresholds for particles punching through the detectors are about 6 MeV/A for protons and α-particles and 7–11 MeV/A for light fragments. The check of the thickness of each Silicon strip, particularly important for the measurements planned with the RCo will be discussed in Section 3.

2.3. The CsI(Tl) scintillators

CsI(Tl) crystals [17] have been chosen as residual energy detectors because they have high density and therefore high stopping power for ions and light charged particles. In addition they are easily machined, not hygroscopic and can suffer without damage relatively strong mechanical shocks and also a relatively high radiation dose. Their density ($4.51\,\mathrm{g/cm^3}$) makes them suitable to stop in few centimeters the ions to be detected. The molar percentage of the Tl atoms in our CsI crystals is in the range of 0.10–0.12% [17]. The light emission is collected by PD and the optical coupling has been obtained by a two-component silicon glue. Since up to 50% of the scintillation light could be lost through the lateral walls of the crystal [18], particular care has been devoted to the treatment of the surfaces, that have been properly polished and wrapped with micro-porous polyvinylidene fluoride membrane [19] and Teflon [20]. PDs have been chosen to read the light output because they require small space, have a good quantum efficiency for the CsI(TI) light emission spectrum, are insensitive to magnetic fields, have a good gain stability and require low bias voltages. However, the output signals are small, compared to those from a photomultiplier, thus requiring a careful signal treatment to optimize the energy resolution. We mounted Hamamatsu S3204-05 [21] ($1.8 \times 1.8\,\mathrm{cm^2}$) PDs, 500 μm thick, selected to have a dark current less than 15 nA.

In order to form an inner and an outer CsI(Tl) ring, for each sector of the apparatus two shapes of the crystal are used. The inner and outer crystals are shown in Fig. 3. The separation of the inner and outer ring corresponds to the separation between the fourth and fifth strips of the preceding silicon detectors.

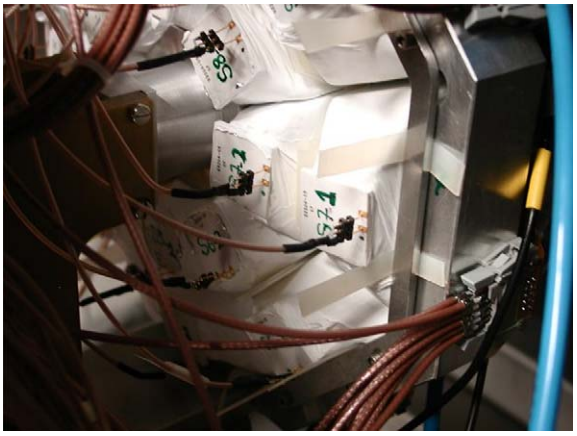

Fig. 3. Picture of the RCo detector from behind, showing the details of the CsI(Tl) crystals, mounted in the holder.

2.4. Electronics and data acquisition system

The electric signals coming from the RCo detectors are treated by standard electronics, very similar to that employed for the GARFIELD array. Each channel consists of a charge preamplifier, a linear amplifier and a peak-sensing ADC. For the three detector types, IC, silicon strips and CsI(Tl) with PD read-out, we use integrated low-noise low-power charge preamplifiers developed by the Electronic Staff of INFN-Milano [12]. The sensitivities and the bias resistors of these charge preamplifiers can be selected among some values by simple soldering contacts on the ceramic board. These parameters were chosen on the basis of the detector type and of the foreseen energetic ranges. For the IC and the CsI crystals, which produce small signals, we used the maximum available gain (90 mV/MeV(Si)) while for the silicon strips we used a sensitivity of 5–10 mV/MeV(Si) to comply with the energy releases up to 0.5–1 GeV. Bias resistors are 10 MΩ for silicon strips and 100 MΩ for the IC and the crystals for which the bias currents are typically under 10 nA.

All the preamplifiers are housed in cooled boxes for operation under vacuum, as shown in Fig. 1.

The signals coming from the preamplifiers are fed to commercial shapers (16—chan. CAEN N568) which, for each channel, give three outputs: two linear Gaussian unipolar pulses (low-*lgp*- and high-*hgp*-gain) for energy determination and a fast signal, *fs*, for triggering and/or timing purposes [22].

The two gains have been used only for the energy signals of the silicon strips with the ratio $R = hgp/lgp \approx 5$. The selected shaping constants have been chosen 3 μs for all kind of detectors. The shaped pulses, both with low and high gain, are peak-sensed by the 32 ch. VME ADC units with FAIR interface [23], designed and built by the Silena factory in collaboration with the Napoli INFN group.

Concerning the *fs*, up to now, we used only the outputs for the 64 silicon strips to build specific RCo triggers via

CFD modules which produce NIM standard pulses. Indeed, the very short flight distances (about 20 cm for the Si-strips), the time properties of the available beams at LNL and not carefully tuning of the fast electronics prevented us from using the *fs* for precise timing purposes. New perspectives in this direction can be opened by the digital sampling devices specifically developed by the NUCL-EX group (see Section 4).

As for any complex many-channel detector employed in long measurement campaigns, the electronics stability is of paramount relevance. The monitoring, during time, of all the energy channels has been performed with the following scheme, designed for the contextual calibration and check of the 180 TDC channels of the GARFIELD array needed for drift-time measurements. An ORTEC-462 Time Calibrator (TC) randomly produces start–stop signals with a selected period in a selected time range. These fast pulses generate a specific trigger (Pulser-Trigger) which can be switched on or off for dedicated pulser runs or for acquiring pulser events also during a physical run together with reaction events (the different events can be then identified during the off-line analysis on the basis of a trigger pattern). While the TC stop signals are sent to the CFD-TDC timing chains (not present for the RCo), the same start–stop intervals are converted in linear squared pulses by an ORTEC-567 TAC. We thus obtain, for each pulser event, a signal pulse which is fed, through specific linear splitters mounted in daisy-chain, to all the test inputs of the preamplifiers of the RCo. Therefore, during a pulser run, we quickly obtain many-peaks TDC spectra and, relevant for the RCo, many-peaks ADC spectra. By means of these spectra, we can follow in time the stability of the energy channels, reconstruct gain changes, study non-linear effects (the linearity of the pulse heights is ensured by the high quality of the pulse generating modules: for the chosen set-up parameters, the integral TAC linearity is better than 1% while the TC nonlinearities are totally negligible). However, we underline that, using this scheme, we cannot easily verify the offset stability. Specific "pedestal" runs have to be performed to get rid of these possible variations. Over the entire beam time of the experiments (about 7 days) we checked that the variation in gain is under 0.2% for all the electronic channels.

3. Performances and operation

All the detectors of the RCo have been separately tested in the laboratory with collimated sources (1 mm in diameter) and the same electronic chain used for in-beam measurements (see Section 2.4).

Fig. 4 shows the spectrum obtained for one of the Silicon strips with a ^{241}Am α-particle source. A three Gaussian fit is also shown where the three peaks correspond in energy and yield to the three decay lines at 5.486 MeV (85.2%), 5.443 MeV (12.6%) and 5.389 MeV (1.3%). The resolution as obtained from the highest peak is about 0.5% FWHM

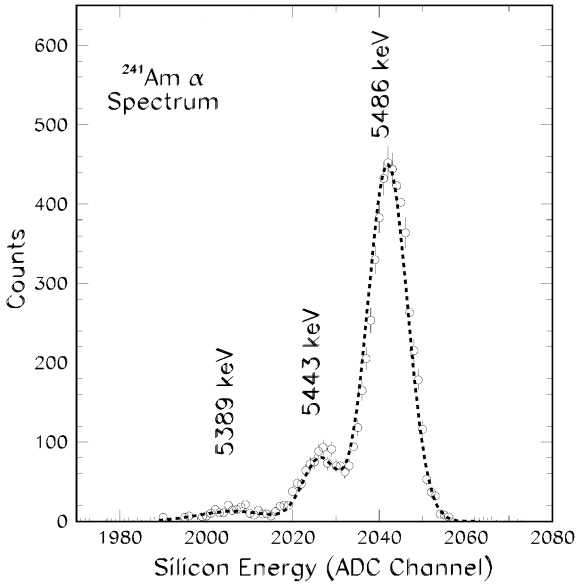

Fig. 4. Energy spectrum of one of the strips of the silicon detectors, obtained with a collimated ^{241}Am α-source.

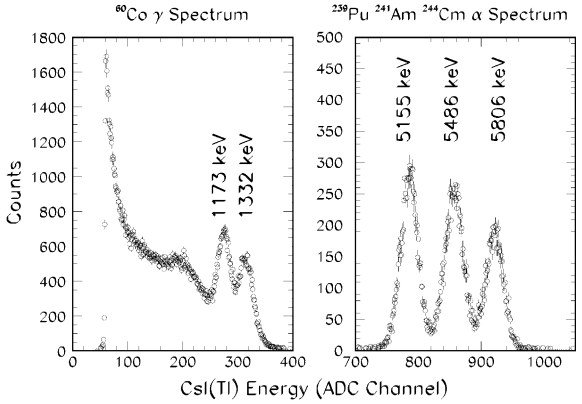

Fig. 5. Energy spectrum of one of the CsI(Tl) crystals, obtained with a collimated ^{60}Co γ-source (left) and a ^{239}Pu, ^{241}Am, ^{244}Cm collimated α-source (right).

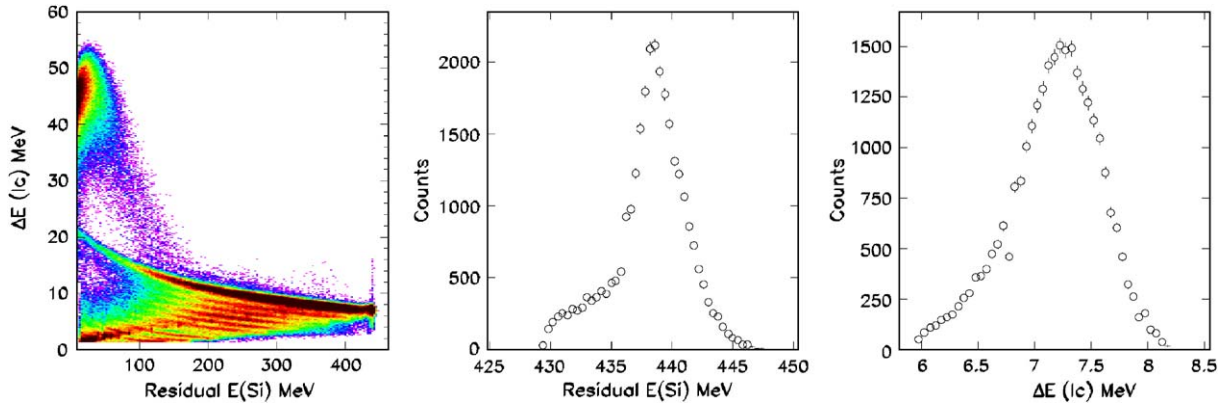

Fig. 6. Left: scatter plot of the IC energy loss versus the Si residual energy for the $^{32}S + ^{64}Ni$ reaction at 14.5 MeV/A, $\theta_{lab} = 9.8^{\circ}$. An upper limit of 200 counts has been set, to make more evident the Z-lines. Middle: residual energy (Si) spectrum of the scattered ^{32}S ions. Right: energy loss (IC) spectrum of the scattered ^{32}S ions. All histograms are summed over the entire experiment.

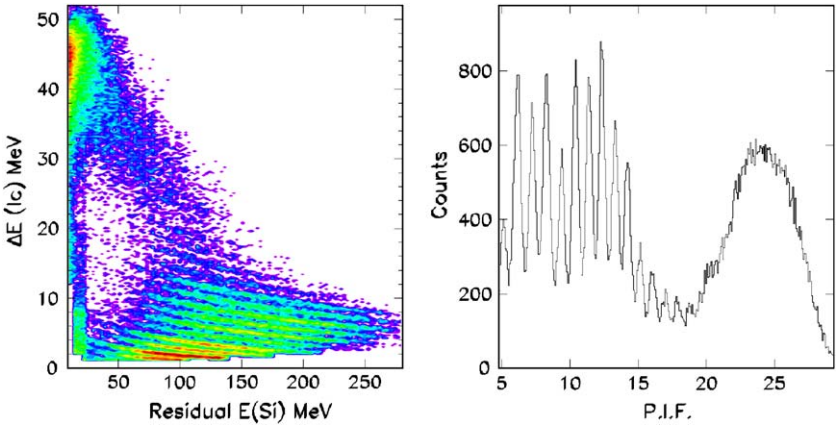

Fig. 7. Left panel: scatter plot of the IC energy loss versus the Si residual energy for the $^{32}S + ^{64}Ni$ reaction at 14.5 MeV/A, for a strip at $\theta_{lab} = 16.7^{\circ}$, summed over the entire experiment. Right panel: corresponding PIF (see text for details).

(~27 keV). It should be noted that the strip resolution shown in Fig. 4 includes the electronic noise of the setup. Taking into account the electronic noise (typically 17 keV, as measured using a precision pulser) we obtain for the intrinsic resolution of the strip a value of about 21 keV (0.4% FWHM).

The CsI(Tl) crystals have been tested with a ^{60}Co γ-source in order to check the response in the bulk crystal (left panel of Fig. 5) and with a ^{239}Pu, ^{241}Am, ^{244}Cm α-particle source in order to measure the energy resolution (Fig. 5, right panel), which resulted in about 4% FWHM.

Since it is well known that the light output of this kind of scintillators depends on the charge, mass and energy of the detected particles, a very careful energy calibration has been performed [24,25] at LNL with several beams at different energies, from protons to Ni. The FWHM energy resolution for the CsI(Tl) has been measured with several beams from ^{7}Li at 3–8 MeV/A to ^{58}Ni at 2–4 MeV/A directly impinging on the crystals during the CsI(Tl) calibration campaign [25]. We obtained resolutions (FWHM) ranging from 2.7% for ^{58}Ni at 239 MeV to 3.3% for ^{7}Li at 23.7 MeV.

Once assembled, the RCo has been tested at LNL in two experiments: $^{32}S + ^{58,64}Ni$ at 14.5 MeV/A and $^{16}O + Sn$ at 15.6 MeV/A. In the first measurement the RCo was placed at 0° with respect to the beam; the grazing angle of the reaction was 8°. The pressure of the IC was 50 mbar. More than 40×10^6 events were collected for both $^{32}S + ^{58,64}Ni$ reactions.

A scatter plot of the energy loss in the IC as a function of the energy deposited in the Si detector is shown in Fig. 6 (left) for a telescope at $\theta_{lab} = 9.8^{\circ}$. Energy calibration of the IC and Si signals were performed through calculated values of the energies released by scattered ^{32}S ions. The energy resolutions for ^{32}S ions with elastic energies, stopped in the silicon detector, are 1.2% FWHM for the residual energy (Si) (Fig. 6 middle panel), including the kinematical spread due to angular extension of the strip and the energy straggling in the preceding IC and 11% FWHM for the energy loss in the IC (Fig. 6 right panel).

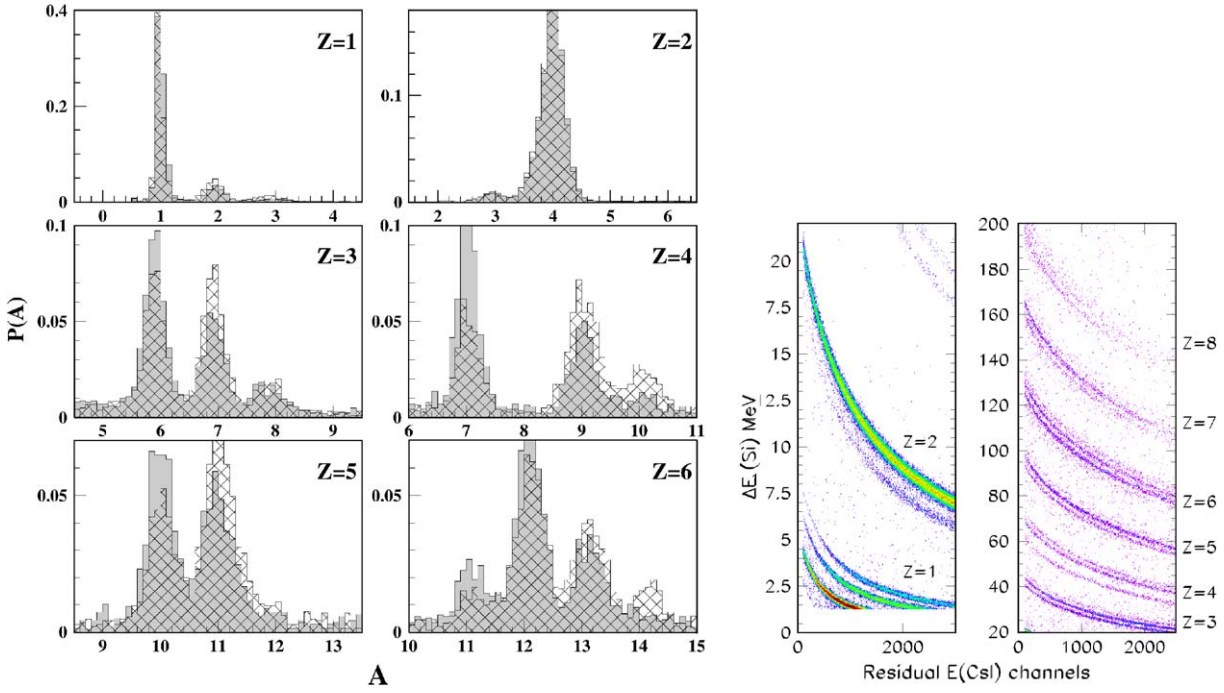

Fig. 8. Left and middle panels: scatter plot of the Si energy loss vs. the CsI residual energy for $^{32}S + ^{64}Ni$ reaction for a strip at $\theta_{lab} = 9.8^{\circ}$, summed over the entire experiment. The zoom in the left panel shows the resolution for $Z = 1$ and $Z = 2$ isotopes. Right panel: mass distributions for $^{32}S + ^{58}Ni$ (gray) and $^{32}S + ^{64}Ni$ (hatched) reactions obtained from the procedure described in the text.

From Fig. 6, it appears that the overall resolution is high enough to obtain good Z separation. The Z lines are clearly visible even beyond the projectile charge. In this plot different regions can be noticed. The more energetic ejectiles, coming from projectiles, populate the low ΔE region of the correlation. Evaporation residue events fill the high-ΔE low-E region where the charges cannot be separated; for these heavy fragments we measured a remarkably low energetic threshold of about 0.7 MeV/A. Finally, we can see an event area bridging the two previous regions which can probably be ascribed to fission events of the heavy residue.

To estimate the Z-resolution and the contamination from adjacent charges through a Particle Identification Function (PIF) analysis [26] and Gaussian deconvolution, we need to de-emphasize elastic and quasi-elastic contributions. Therefore we show in Fig. 7 the scatter plot of the IC energy loss versus the Si residual energy for a strip at $\theta_{lab} = 16.7^{\circ}$. In the right panel we show the corresponding PIF. In the region of charges smaller than 20, peaks in the PIF show the capability of resolving fragment charge. In particular, for $Z \leqslant 14$ a Z resolution of the order of 0.6 charge units FWHM and a peak to noise ratio of the order of four suggest a contamination from adjacent charges smaller than 4%. As far as charges larger than 20 are concerned, we can only assign to these fragments a raw charge value. On the other hand, the use of a low pressure for the IC allows to lower the detection thresholds also for heavy fragments and

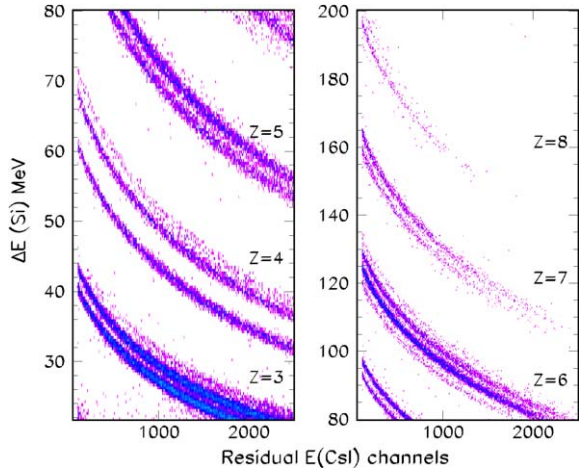

Fig. 9. Scatter plot of the Si energy loss vs. the CsI residual energy for strips belonging to the same sector. The histograms are summed over all the events of the $^{32}S + ^{58}Ni$ and $^{32}S + ^{64}Ni$ reactions.

evaporation residue but give access to the energetic region under 1 MeV/A where the Z^2A dependence of the energy loss is destroyed by nuclear collisions and effective-charge effects.

When the ions punch through the silicon detector, mass identification, at least for IMF charges up to $Z = 8$, can be obtained from the correlation between the energy loss in the Si strip and the residual energy in the CsI scintillator

(see Fig. 8 left). Very good identification starting from protons, deuterons, tritons up to the oxygen isotopes clearly appears from the figure.

In order to make a quantitative analysis for fragment identification in charge and mass, the procedure introduced in Ref. [26] has been used. On the ΔE–E scatter plot some points on the lines of well-defined isotopes (as ^{1}H, ^{4}He, ^{7}Li, ^{7}Be, ^{11}B, ^{12}C) are sampled. A minimization routine determines, for each detector, the set of parameters of a "Bethe-Bloch like" function able to reproduce the energy loss of the sampled points. Then, event by event, from the measured values of the $\Delta E, E$, an algorithm calculates the charge and the mass for each detected charged product, basing on the distances from the (A, Z) lines calculated through the previously determined parameters. A real number is extracted for the mass and the difference from the integer takes into account the distance from the closest line, giving indication of the resolution on the mass determination. An example of the results of this procedure is shown in the right panel of Fig. 8, where the mass distributions obtained for $^{32}S + ^{58}Ni$ and for $^{32}S + ^{64}Ni$ reactions are displayed, also showing the isospin dependence of isotope production. Isotopes from hydrogen to carbon are clearly separated [26]. Peak-to-valley ratios for the dominant isotopes are approximately a factor of four, demonstrating the good isotopic resolution attained. In some of the telescopes isotopes up to oxygen are well identified.

Since one of the goals of the $^{32}S + ^{58,64}Ni$ experiment is the mass identification of light charged particle and fragments and the measurement of their total energy, it is very important to experimentally verify the uniformity of the Si thickness.

Indeed one of the methods we employed to trace-back, event by event, the initial energy of a (A, Z) isotope, punching through the IC and the silicon detectors and stopped in the CsI(Tl) crystal, makes use of energy loss tables, by assuming that all the active and dead layer thicknesses are well known. Energy-loss calculations showed that by mixing Si thicknesses different by 5 μm (10 μm) a complete lack of mass resolution should be observed, at the level of oxygen (carbon) isotopes.

Therefore, we have added the scatter plots of the Si energy loss vs. the CsI residual energy for the strips belonging to the same Si sector (Fig. 9). We have found that the very good mass separation obtained after this sum is a proof of the uniformity of all the active and dead layers at least within 1–2%.

The quality of the energy calibration and the granularity of the RCo can be tested by the correlation functions of the relative momentum between selected pairs of isotopes.

One can define [27] the two-fragment relative momentum correlation function as

$$1 + R(q_{\mathrm{rel}}) = C\,\frac{Y(q_{\mathrm{rel}})}{Y_{\mathrm{back}}(q_{\mathrm{rel}})}$$

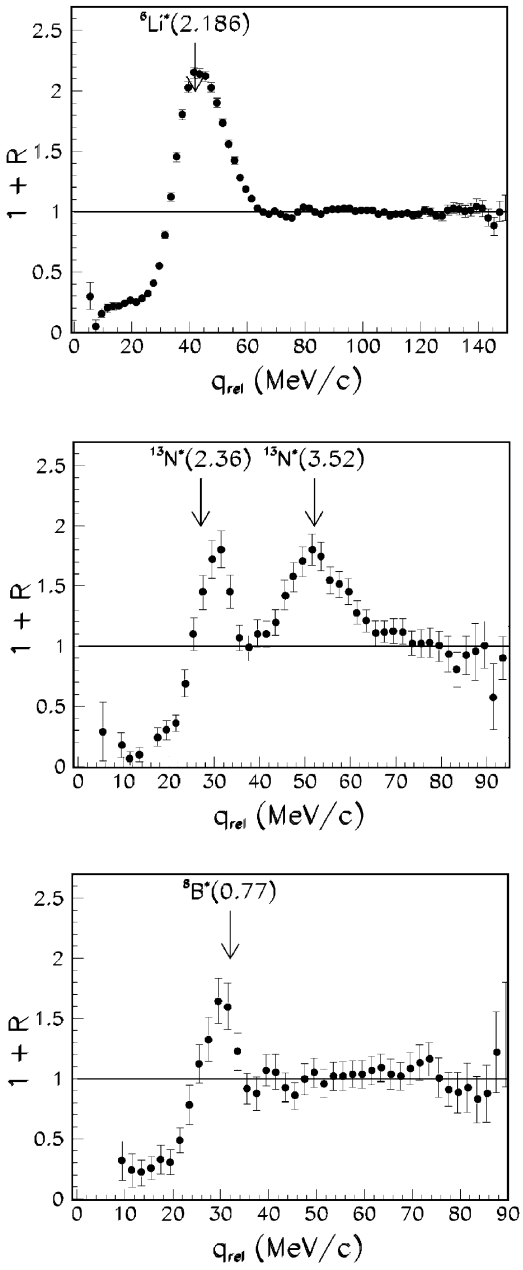

Fig. 10. Correlation functions of the relative momentum in $^{32}S + ^{64}Ni$ reaction at 14.5 MeV/A: top panel: d-α; middle panel: p-^{12}C; bottom panel p-^{7}Be.

where $q_{\mathrm{rel}} = |\vec{q}_i - \vec{q}_j|$ is the value of the relative momentum of isotopes i and j, $q_{i,j} = A_{i,j}\vec{v}_{i,j}$ are the individual momenta, A_i and A_j the masses and $\vec{v}_i$ and $\vec{v}_j$ the velocities of the two isotopes. $Y(q_{\mathrm{rel}})$ and $Y_{\mathrm{back}}(q_{\mathrm{rel}})$ are the coincidence and background yields for fragment pairs of relative momentum q_{rel} and $C = N_{\mathrm{back}}/N_{\mathrm{coinc}}$ where N_{coinc} and N_{back} are the total number of coincidence and background pairs. The background yield is constructed by means of the mixed event technique.

All the correlation functions of isotope pairs, expected to lead to the observation of resonances of the *compound* fragment were calculated over the entire experiment.

A high number of resonant states has been observed. In Fig. 10 we show few examples of correlation functions: deuteron–α, proton–carbon and proton–beryllium, where peaks due to resonances clearly appear [10]. Other examples are shown in Ref. [11]. Arrows in Fig. 10 indicate the expected value of the relative momentum, in agreement with our experimental findings. We are confident that this kind of high quality correlation functions will allow us to get information on the abundance of well-defined excited primary fragments at an early stage of the reaction. This is indeed a direct way to get information on primary partitions and, consequently, to achieve a better determination of temperatures from isotope abundance, once the fragmenting source has been characterized. In other words, interferometric studies of this type allow to estimate the IMF multiplicities at the primary stage, as well as to build isotope and excited state thermometers to obtain information on the temperature of the decaying system before secondary decays.

This kind of analysis is a powerful tool also in other fields, like in astrophysics. The formation and the decay of excited states of light nuclei in the nuclear medium, as it occurs in stellar processes, are not well known. In Fig. 10 (middle and left panels) an example of such a formation is given, where p–^{12}C and p–^{7}Be correlation functions indicate the production of ^{13}N* and ^{8}B* excited states in the nuclear medium.

4. Perspectives

Improvements on the use of the RCo detector in future measurements will be achieved by using the digital sampling electronics especially designed [28] for the NUCL-EX experiments [8] and recently tested with some of the modules [29].

In the ^{16}O + Sn at 15.6 MeV/A experiment the RCo has been placed at a large angle in a parasitic and independent measurement, to test the pulse-shape analysis of the CsI(Tl) and silicon signals with the new electronics. The IC has been kept empty, therefore the Silicon detector acts as ΔE detector and the CsI(Tl) crystal as stopping detector.

The aim was to compare the digital sampling electronics with the standard one as far as energy measurements and mass identification are concerned and, in addition, to explore the pulse-shape capability of the new sampling devices when used with CsI.

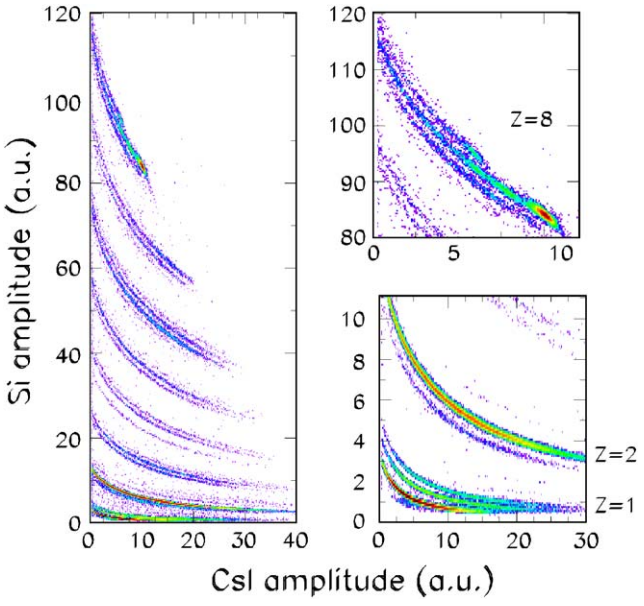

Fig. 11. Si–CsI scatter plot obtained with digital sampling electronics for a telescope of the RCo for the ^{16}O + Sn reaction at 15.6 MeV/A.

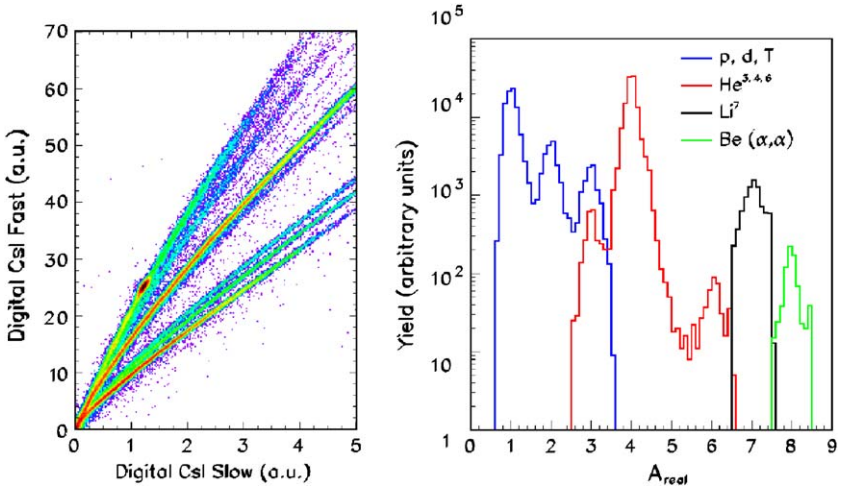

Fig. 12. Left panel: fast–slow signals from the CsI(Tl) crystals of the RCo obtained with the digital electronics for the ^{16}O + Sn reaction at 15.6 MeV/A. Right panel: mass distributions obtained from fast–slow signals of the left panel data.

In Fig. 11 results obtained with a prototype are shown (the details of the employed digital processing system are reported in Ref. [29]).

Concerning energy resolution of the Si and CsI(Tl) detectors for elastically scattered ^{16}O ions, stopped in the CsI(Tl) crystal, they resulted 2% and 9% FWHM, respectively, including the kinematical spread due to the angular extension of the strip, the energy straggling in the mylar windows and in the detectors themselves.

The mass separation is even better than the one obtained with the standard analogical treatment of the signals. These encouraging results make us confident that it will be also possible to extend the mass identification to ions heavier than the oxygen isotopes.

As far as the pulse-shape analysis with CsI(Tl) is concerned, the digital sampling devices will allow the identification of light charged products (up to $Z \approx 4$) with high energies, which, due to the low energy deposition in the IC and Si stages, cannot be resolved with standard $\Delta E - E$ techniques. As an example, Fig. 12 shows the plot of the fast vs. the slow components of the scintillation and the corresponding mass spectrum obtained by an event by event identification [29]. In this case also peak-to-valley ratios for the dominant isotopes are at least a factor of four, demonstrating the good isotopic resolution attained.

5. Conclusions

The design and the performances of a complex detector, based on IC–Si–CsI(Tl) telescopes, have been presented. The array meets the criteria of well characterizing the light charged particles and fragments emitted in heavy ion reactions with projectiles of approximately 10–30 MeV/A incident energy. This array, coupled to the GARFIELD apparatus, is suitable for the measurements proposed by the INFN NUCL-EX group [8], which aims to study both thermodynamic and dynamic aspects in heavy ion reactions, for $A \approx 100$ systems.

The RCo allows to detect and identify light particles and fragments with very low energy thresholds and good energy, charge and mass resolutions. The performances of newly designed dedicated prototypes of digital sampling electronics will significantly improve the performances of the apparatus both for energy determination and for particle identification. The digital electronics will be firstly used for the pulse-shape analysis of the CsI(Tl) scintillators and for energy measurements with silicon detectors. In the future we will try to extend digital pulse-shape analysis also to the signals of the RCo silicon strips in order to possibly identify the masses at least for relatively light fragments stopped in the Si detector, thus allowing for a better determination of the isospin of the sources.

In future applications, in order to reduce energy thresholds for mass identification of fragments, a further thinner annular silicon detector is planned to be placed between the ionization chamber (IC) and the 300 μm silicon detector. We also plan to rotate the low-mass aluminum support of the silicon detector, in order to place each Si sector covering one half of two adjacent ICs and CsI(Tl) sectors, thus increasing the granularity of the array.

Acknowledgements

We are grateful to C. Baiocchi, R. Bassini, A. Boiano, C. Boiano, U. Carcassi, L. Costa, P. Del Carmine, M. Giacchini, M. Negrato, M. Ottanelli, A. Paolucci and G. Tobia for their skillful assistance.

We are indebted to Dr. U. Abbondanno for encouraging discussions, hints and a careful reading of the manuscript.

This work was supported in part by grants of Alma Mater Studiorum (Bologna University).

References

[1] P. Chomaz, Nucl. Phys. A 685 (2001) 274;
P. Chomaz, Proceedings of INPC2001, AIP Proceedings, vol. 610, 2002, p. 167.
[2] See, for instance: <www.ganil.fr/eurisol/Final_Report/APPENDIX-E.pdf>
[3] B. Davin, et al., Nucl. Instr. and Meth. A 473 (2001) 302.
[4] T. Paduszynsky, et al., Nucl. Instr. and Meth. A 547 (2005) 464.
[5] F. Gramegna, et al., Nucl. Instr. and Meth. A 389 (1997) 474.
[6] F. Gramegna, et al., 2004 IEEE Nuclear Science Symposium, Rome, 16–22 October, 2004.
[7] F. Gramegna, et al., Acta Phys. Polonica B 36 (2005) 1155.
[8] See, for instance, <www.bo.infn.it/nucl-ex>
[9] U. Abbondanno, et al., LNL 2004 Annual Report, LNL-INFN(REP)-204/2004 ISBN 88-7337-008-X, p. 39; <www.lnl.infn.it/%7Eannrep/read_an/2004/index_2004.html>
[10] M. Bruno, et al., Proceedings of the Fifth Italy–Japan Symposium, Naples, November 3–7, 2004, in: G. La Rana, C. Signorini, S. Shimoura (Eds.), Recent Achievements and Perspectives in Nuclear Physics, World Scientific, in press.
[11] M. D'Agostino, M. Bruno, F. Gulminelli, F. Cannata, Ph. Chomaz, G. Casini, E. Geraci, F. Gramegna, A. Moroni, G. Vannini, Nucl. Phys. A 749 (2005) 55.
[12] R. Bassini, C. Boiano, S. Brambilla, I. Iori, M. Malatesta, A. Moroni, Nucl. Instr. and Meth. A 305 (1991) 449;
R. Bassini, C. Boiano, S. Brambilla, A. Pullia, IEEE Trans. Nucl. Sci. 49 (5) (2002).
[13] S. Brambilla, et al., in preparation.
[14] Manufactured by Canberra Industries INC.
[15] Produced by STESALIT AG (Switzerland). It is a synthetic material reinforced with glassfibre, <www.stesalit.com/e_5_4.cfm>
[16] L. Bardelli, M. Bini, G. Poggi, N. Taccetti, Nucl. Instr. and Meth. A 491 (2002) 244.
[17] Supplied by Scionix—The Netherlands.
[18] I. Iori, et al., Nucl. Instr. and Meth. A 325 (1993) 458.
[19] Millipore Inc. <www.millipore.com>
[20] F. Tonetto, U. Abbondanno, M. Chiari, P.M. Milazzo, L. Travaglini, Nucl. Instr. and Meth. A 420 (1999) 181.
[21] Supplied by HAMAMATSU Italia SRL.
[22] R. Bassini, C. Boiano, S. Brambilla, M. Malatesta, I. Iori, A. Moroni, Nucl. Instr. and Meth. A 327 (1993) 535;
R. Bassini, C. Boiano, S. Brambilla, M. Malatesta, IEEE Trans. Nucl. Sci. NS-42 (4) (1995).
[23] A. Ordine, A. Boiano, E. Vardaci, A. Zaghi, A. Brondi, FAIR: a new fast trigger and readout bus system, IEEE Trans. Nucl. Sci. NS-45 (3) (1998).

[24] U. Abbondanno, et al., Nucl. Instr. and Meth. A 488 (2002) 604.
[25] G. Casini, et al., LNL 2004 Annual Report, LNL-INFN(REP)-204/2004 ISBN 88-7337-008-X, pp. 212–214; <www.lnl.infn.it/%7Eannrep/read_an/2004/index_2004.html>, Nucl. Instr. and Meth., to be submitted.
[26] N. Le Neindre, et al., Nucl. Instr. and Meth. A 490 (2002) 251.
[27] R. Trockel, et al., Phys. Rev. Lett. 59 (1987) 2844;
Y.D. Kim, R.T. de Souza, D.R. Bowman, N. Carlin, C.K. Gelbke, W.G. Gong, W.G. Lynch, L. Phair, M.B. Tsang, F. Zhu, S. Pratt, Phys. Rev. Lett. 67 (1991) 14.
[28] M. Bini, et al., in preparation.
[29] L. Bardelli, G. Poggi, M. Bini, G. Pasquali, N. Taccetti, Nucl. Phys. A 746 (2004) 272.